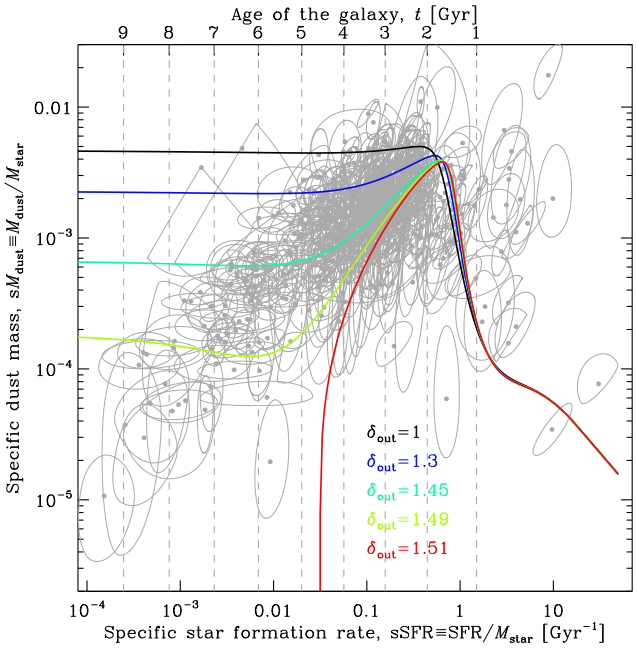

Fig. 15. Effect of outflow on the s$M_{\rm dust}$–sSFR relation. The data are identical to panel c of Fig. 14. The colored lines represent our dust evolution model. We have fixed all the parameters close to their maximum a posterior values, except the outflow rate, $\delta_{\rm out}$: $\tau_{\rm SFH} = 0.8$ Gyr, $\psi_0 = 40\,M_\odot\,{\rm yr}^{-1}$, $\delta_{\rm in} = 1.0$, $\delta_{\rm SN} = 0.01$, $\epsilon_{\rm grow} = 4500$, and $m_{\rm gas}^{\rm dest} = 1200\,M_\odot$/SN. The different lines correspond to different values of $\delta_{\rm out}$. The top axis displays the age of the galaxy corresponding to the particular SFH of the model run. We have used a Salpeter (1955) IMF.

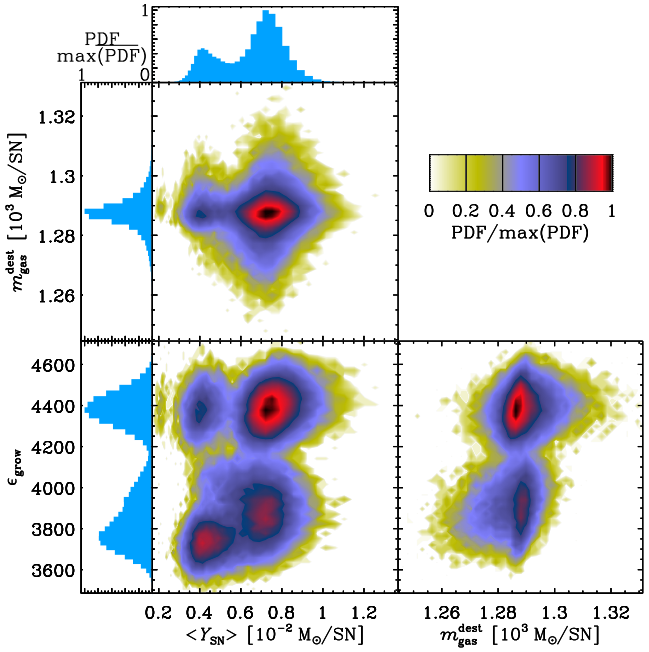

Fig. 16. Posterior distribution of the tuning parameters, assuming a Salpeter (1955) IMF. The *three central panels* with colored contours display the bidimensional posterior PDF of pairs of parameters, marginalizing over all the other ones. The *three margin plots* show the posterior PDF of each tuning parameter. The PDFs are scaled (divided by their maximum). The displayed ranges encompass every single parameter draw after burn-in.

sample. In Sect. 4.1.3, we have extensively discussed the different systematic effects that could have biased these estimates. If some of these effects are, at some point, proven to be relevant, our inference of $\langle Y_{\rm SN}\rangle$ would have to be revised accordingly. To first order, the SN dust yield is proportional to the dustiness of the lowest metallicity objects:

$$\langle Y_{\rm SN}\rangle \simeq 0.007\,M_\odot/{\rm SN} \times \frac{Z_{\rm dust}({\rm I\,Zw\,18})}{1.9\times10^{-6}}. \quad (16)$$

We also notice that $\delta_{\rm SN}$ and $m_{\rm gas}^{\rm dest}$ are peaking at the tail of their prior. It means our data carries a large weight evidence. It also means the values we infer are probably an upper limit for $\delta_{\rm SN}$ and a lower limit for $m_{\rm gas}^{\rm dest}$. Since $m_{\rm gas}^{\rm dest}$ and $\epsilon_{\rm grow}$ are correlated, our inference of $\epsilon_{\rm grow}$ is also probably a lower limit. We have estimated in Sect. 4.1.3 that the dustiness of ELMGs could have been underestimated by a factor of at most ≃4.25, the conservative conclusions we can draw from our analysis are thus that: $\langle Y_{\rm SN}\rangle \lesssim 0.03\,M_\odot$/SN; $\epsilon_{\rm grow} \gtrsim 3000$; $m_{\rm gas}^{\rm dest} \gtrsim 1200\,M_\odot$/SN.

The SFH-related parameters. Figure 17 displays the corner plot of the five parameters controlling the individual SFH of each galaxy. The displayed PDF is the posterior of the parameters of every galaxy. There is a relatively large scatter of these parameters, implying that our different galaxies have different SFHs. We note that the interpolation between models does not produce a perfectly smooth distribution. The edges of our model grid are visible in this corner plot. This does not however impact the results as our grid samples well enough the PDF.

5.3.2. The dust evolution timescales

It is possible to estimate the posterior PDF of the dust evolution timescales of each galaxy, from the inferred parameters of Figs. 16 and 17, using Eqs. (11)–(14). Figure 18 displays these timescales as a function of metallicity. Although there is some scatter due to the different SFH and age of galaxies in a given metallicity bin, we note that these timescales evolve.

The SN II dust condensation timescale (panel a of Fig. 18) is around $\tau_{\rm cond} \simeq 100$ Myr for ELMGs, implying that dust can be dominated by stardust in this regime. It rises up to $\tau_{\rm cond} \simeq 1000$ Gyr around solar metallicity, indicating this process is not sufficient to account for all ISM dust in evolved systems.

The grain growth timescale (panel b of Fig. 18) is quite scattered. It starts around $\tau_{\rm grow} \simeq 1$ Gyr in the ELMG regime and decreases down to $\tau_{\rm grow} \simeq 50$ Myr around solar metallicity. The average value of our sample at 12 + log(O/H) ≥ 8.5 is $\tau_{\rm grow} \simeq 45$ Myr. It is another way to show that dust formation is dominated by grain growth around solar metallicity.

The SN II dust destruction timescale (panel c of Fig. 18) is also scattered but stays around $\tau_{\rm dest} \simeq 300$ Myr across our metallicity range.

The Milky Way value displayed in the three panels is consistent with the cloud of points in the highest metallicity domain.

There is a common misconception that dust destruction by SN II blast waves is unimportant at early-stages, because the dustiness is so low that few grains are destroyed by a single SN II. However, we show here that this is not the case as: (i) the SN II rate is on average higher at low-metallicity; (ii) the fraction of grains destroyed by a single SN II is dustiness-independent.

5.3.3. Sensitivity to the IMF

As we discussed in Sects. 2.2.3 and 2.2.4, the main uncertainty on our estimated $M_\star$ and SFR comes from our IMF assumptions. Those were derived with a Salpeter (1955) IMF. Here, we